Quaternary Science Reviews 137 (2016) 33–44

Contents lists available at ScienceDirect

Quaternary Science Reviews

journal homepage: www.elsevier.com/locate/quascirev

Quantitative woody cover reconstructions from eastern continental Asia of the last 22 kyr reveal strong regional peculiarities

Fang Tian [a, b], Xianyong Cao [a, *], Anne Dallmeyer [c], Jian Ni [a, d], Yan Zhao [e], Yongbo Wang [a], Ulrike Herzschuh [a, b]

[a] Alfred Wegener Institute Helmholtz Centre for Polar and Marine Research, Research Unit Potsdam, Telegrafenberg A43, Potsdam 14473, Germany
[b] Institute of Earth and Environment Science, University of Potsdam, Karl-Liebknecht-Str. 24, Potsdam 14476, Germany
[c] Max Planck Institute for Meteorology, KlimaCampus, Bundesstrasse 53, Hamburg 20146, Germany
[d] State Key Laboratory of Environmental Geochemistry, Institute of Geochemistry, Chinese Academy of Sciences, Guanshui Road 46, Guiyang 550002, China
[e] Institute of Geographic Sciences and Natural Resources Research, Chinese Academy of Sciences, Datun Road 11, Beijing 100101, China

ARTICLE INFO

Article history:
Received 1 October 2015
Received in revised form
30 January 2016
Accepted 1 February 2016
Available online xxx

Keywords:
Pollen
AVHRR
Modern analogue technique
Quantitative reconstruction
East Asian summer monsoon

ABSTRACT

We present a calibration-set based on modern pollen and satellite-based Advanced Very High Resolution Radiometer (AVHRR) observations of woody cover (including needleleaved, broadleaved and total tree cover) in eastern continental Asia, which shows good performance under cross-validation with the modern analogue technique (all the coefficients of determination between observed and predicted values are greater than 0.65). The calibration-set is used to reconstruct woody cover from a taxonomically harmonized and temporally standardized fossil pollen dataset (including 274 cores) with 500-year resolution over the last 22 kyr. The spatial range of forest has not noticeably changed in eastern continental Asia during the last 22 kyr, although woody cover has, especially at the margin of the eastern Tibetan Plateau and in the forest-steppe transition area of north-central China. Vegetation was sparse during the LGM in the present forested regions, but woody cover increased markedly at the beginning of the Bølling/Allerød period (B/A; ca. 14.5 ka BP) and again at the beginning of the Holocene (ca. 11.5 ka BP), and is related to the enhanced strength of the East Asian Summer Monsoon. Forest flourished in the mid-Holocene (ca. 8 ka BP) possibly due to favourable climatic conditions. In contrast, cover was stable in southern China (high cover) and arid central Asia (very low cover) throughout the investigated period. Forest cover increased in the north-eastern part of China during the Holocene. Comparisons of these regional pollen-based results with simulated forest cover from runs of a global climate model (for 9, 6 and 0 ka BP (ECHAM5/JSBACH ~1.125° spatial resolution)) reveal many similarities in temporal change. The Holocene woody cover history of eastern continental Asia is different from that of other regions, likely controlled by different climatic variables, i.e. moisture in eastern continental Asia; temperature in northern Eurasia and North America.

1. Introduction

Today, climate change and human activities are known to strongly affect woody cover, especially in arid and semi-arid areas where arboreal taxa are growing at the edge of their climatic niche (Tarasov et al., 2007; Liu and Tian, 2010; Ni et al., 2014). Broad-scale quantitative reconstructions of past woody cover based on palynology are necessary for understanding the present-day distribution of forests and for disentangling their driving forces, and they can also provide a useful benchmark for assessing the results of vegetation modelling research. Broad-scale changes in Quaternary woody cover in North America (Williams, 2003; Williams et al., 2011) and northern Eurasia (Tarasov et al., 2007; Williams et al., 2011) have been reconstructed using continental and regional pollen databases combined with satellite-based Advanced Very High Resolution Radiometer (AVHRR) observations of woody cover (DeFries et al., 1999) that find the closest analogues for fossil pollen samples from modern pollen datasets. AVHRR data provide a powerful tool to reconstruct woody cover gradients using analogue-based approaches (Williams and Jackson,

* Corresponding author.
E-mail addresses: Xianyong.Cao@awi.de, cxyhebtu@sohu.com (X. Cao).

http://dx.doi.org/10.1016/j.quascirev.2016.02.001
0277-3791/

2003). Williams (2003) and Tarasov et al. (2007) suggest that climate is the major driver of woody cover change. Having similar data on past land-cover changes for eastern continental Asia (mainly China, Mongolia, and southern Siberia) is of particular interest because of their more complicated climate and vegetation systems, but to date, few studies on land-cover change in this region have been made. Ren (2007) presents changes in forest cover in China during the Holocene using a greater than 40% arboreal pollen limit, but the various arboreal pollen taxa have different pollen representation factors (e.g. Xu et al., 2007; Cao et al., 2015). Zheng et al. (2010) established a pollen calibration-set for woody cover reconstruction. Tarasov et al. (2007) reconstructed the spatial pattern of woody cover for the last glacial maximum (LGM: ~21 ka BP) in northern Eurasia (mainly Siberia and Mongolia) and the temporal changes of woody cover during the late glacial and Holocene using four selected fossil pollen records. Liu et al. (2013) reconstructed regional vegetation cover changes quantitatively based on 15 fossil pollen spectra for north-central China. Ni et al. (2014) reconstructed biome changes in China over the last 22 kyr based on numerical pollen data. These studies provide some primary information on the broad-scale vegetation changes in eastern continental Asia; however, for a more accurate picture of woody cover change, large spatial-scale quantitative studies are necessary.

In this study, we employ a taxonomically harmonized and temporally standardized fossil pollen dataset (Cao et al., 2013) covering the last 22 kyr with 500-year temporal resolution, focusing on eastern continental Asia. We reconstruct needleleaved, broadleaved and total tree cover densities based on a modern pollen dataset (Cao et al., 2014) and AVHRR data, by quantifying the relationship between the palynological and AVHRR-estimates of woody cover, and test the accuracy of regional woody cover reconstructions. We apply the Modern Analogue Technique (MAT) to fossil pollen records to reveal the spatial and temporal changes of woody cover since 22 ka BP; and validate the reconstructions with simulation results from a global climate model for 9, 6 and 0 ka BP (Dallmeyer et al., 2013). The model is also used to detect the potential driving forces of any changes. Our aims are to (1) evaluate the quality of the calibration and reliability of the reconstructions; (2) characterize the overall woody cover change for certain intervals; (3) extract regional differences in the temporal evolution of woody cover; (4) identify the major driver of woody cover change; and (5) compare our reconstruction to general trends of woody cover change from other (sub-)continents.

2. Study area

In the study area (eastern continental Asia, 18°–55°N, 70°–135°E), vegetation follows a south-east–north-west precipitation gradient, changing from a moist coastal forest zone, via steppe, to desert. The eastern part of the study area reflects the influence of the East Asian Summer Monsoon (Fang et al., 1996), allowing dense forest to develop. The natural forest type in the eastern part of the study area consists of tropical rainforest and seasonal rainforest (south of ~23°N; mean annual temperature (T_{ann}): 21–26 °C; mean annual precipitation (P_{ann}): 1200–2200 mm), subtropical evergreen broadleaved forest (23°–32°N) and warm-temperate deciduous forest (32°–40°N) (T_{ann}: 14–21 °C; P_{ann}: 1000–1800 mm), temperate mixed conifer-deciduous broadleaved forest (40°–50°N; T_{ann}: 0–14 °C; P_{ann}: 500–1000 mm), and boreal conifer forest (north of ~50°N; T_{ann}: −5 to −1 °C; P_{ann}: 400–600 mm). In the north-western part of the study area, which is dominated by westerlies, the alpine coniferous forests are limited to mountainous areas. Many plains in the eastern part of the study area are farmed, and forests have only survived in mountainous areas. Deciduous broadleaved taxa (e.g. *Quercus*, *Betula*, *Alnus*, *Ulmus, Juglans*) and evergreen needleleaved taxa (e.g. *Picea*, *Pinus, Abies*) are regionally widespread, while evergreen broadleaved taxa (e.g. *Castanopsis*, *Cyclobalanopsis, Fagus*) are restricted to the tropical and subtropical areas.

3. Data and methods

3.1. Modern and fossil pollen data

The modern pollen dataset used here consists of 2626 pollen spectra from China and Mongolia (Fig. 1) compiled by Cao et al. (2014). We excluded 117 samples from marine (and coastal areas) and 98 samples from lakes with an area larger than 1 km^2 (as neither have local vegetation, but might have high arboreal pollen percentages), following the experience of previous studies (e.g. Williams, 2003; Tarasov et al., 2007), leaving us with 2411 spectra.

A fossil pollen dataset (Cao et al., 2013) with 271 records was employed to reconstruct past woody cover changes since 22 ka BP at a 500-year resolution in eastern continental Asia. For the 271 records, pollen percentages were standardized, pollen names harmonized, an age-depth model re-established, and pollen abundance interpolated for each 500-year interval. Further details are described in Cao et al. (2013). In this study, we added three new records with raw pollen percentage data: Lake Donggi Cona (35.5°N, 98.5°E, 4090 m a.s.l.; Wang et al., 2014) from the eastern part of the Tibetan Plateau, Lake Sumxi Co (34.6°N, 84.2°E, 5059 m a.s.l.; Campo and Gasse, 1993) from the western margin of the Tibetan Plateau, and Lake Bayan Nuur (90.9°N, 48.8°E, 1576 m a.s.l.; Krengel, 2000) from north-west Mongolia. These 274 pollen records evenly cover the major vegetation zones of the study area (Fig. 1).

3.2. AVHRR data

The modern estimates of four cover types (needleleaved, broadleaved, deciduous and evergreen tree cover) were produced from AVHRR observations for 1992 to 1993 (DeFries et al., 2000) in which each 1 × 1 km pixel was described as a percent mixture of several vegetation-cover categories, varying from 0% to 80%. For data extraction, Williams and Jackson (2003) suggest that search window half-widths between 25 and 100 km can best capture the pollen and AVHRR forest cover estimates, which is also consistent with studies of pollen source areas for lakes and mires (Bradshaw and Webb, 1985; Jackson, 1990; Sugita, 1993; Xu et al., 2012). In our study, we used a square search window with a half-width of 50 km to assign AVHRR-based estimates and modern pollen data by centring the window on each modern-pollen site and averaging AVHRR-based estimates from all pixels within the window using ArcGIS 10 software. We recalculated the total tree cover by summing the broadleaved and needleleaved tree cover for each modern pollen site. Due to a strong correlation between broadleaved and deciduous cover, and between needleleaved and evergreen cover (Appendix 1), we only present and discuss the results for broadleaved, needleleaved and total tree cover, while the results for deciduous and evergreen tree cover are in the supplementary material (Appendix 2 and 3).

3.3. Numerical analysis

In our modern pollen dataset, 1180 sites (ca. 49% of the 2411 sites) have ≤5% total tree cover. As an uneven distribution of sites along a gradient will strongly impact transfer function performance (Telford and Birks, 2011), we established a subset of modern pollen comprising 1531 sites including 1231 sites with total tree cover >5% plus 300 sites randomly selected from the 1180 sites with cover

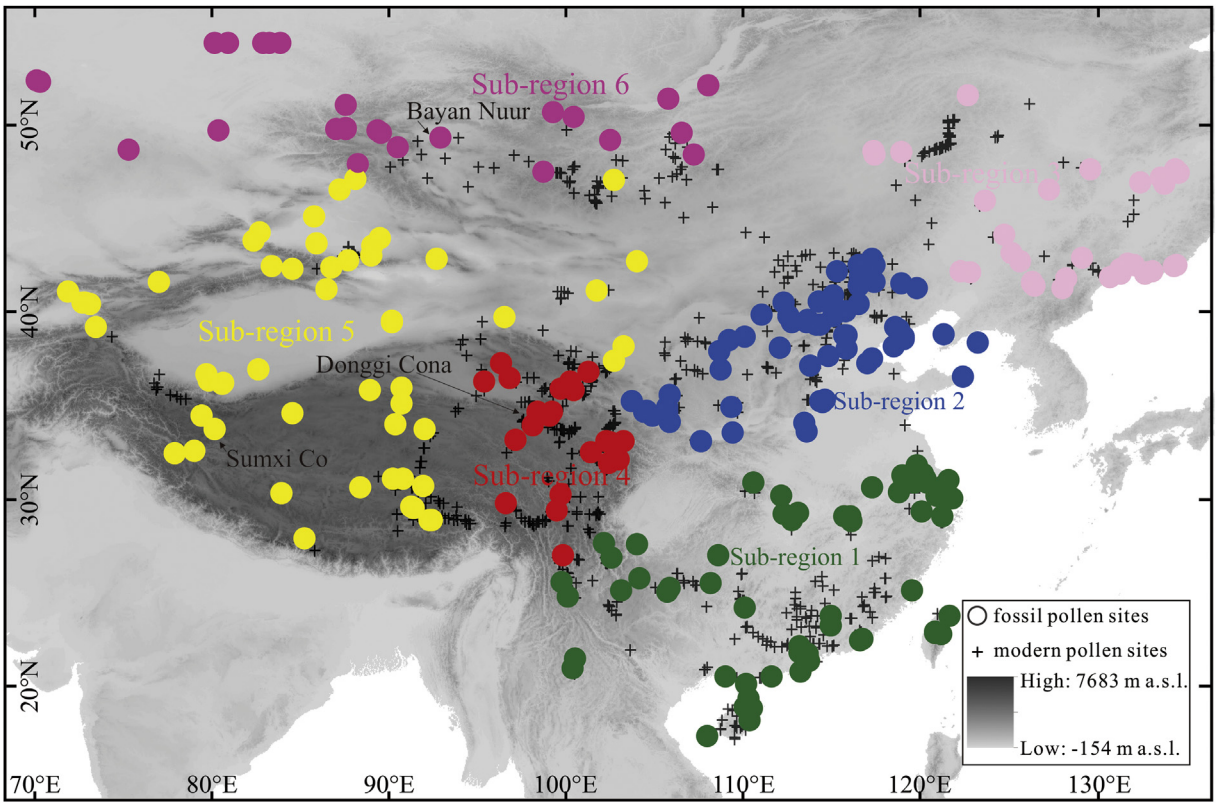

Fig. 1. The distribution of 1531 modern pollen sites (plus signs) and 274 fossil pollen records (filled circles; six sub-regions: 1, south-eastern China; 2, north-central China; 3, north-eastern China and Russia Far East; 4, eastern Tibetan Plateau; 5, arid central Asia; 6, northern Mongolia and southern Siberia) in eastern continental Asia. The three lake names indicate the locations of the new added pollen records. (For interpretation of the references to colour in this figure legend, the reader is referred to the web version of this article).

≤5% (using the simple function in R 3.0.2; R Core Team, 2012) to even out the imbalance.

To reconstruct woody cover changes over the last 22 kyr, we applied the pollen/AVHRR-based Modern Analogue Technique (MAT) and weighted averaging partial least squares (WA-PLS; detailed information in Appendix 3) using the rioja package (Juggins, 2012) in R 3.0.2 (R Core Team, 2012) to a set of pollen assemblages from China and Mongolia. MAT estimates of woody cover were derived from weighted averages of modern woody cover variables of the five closest analogues, using the squared-chord distance to quantify similarity (Overpeck et al., 1985; Prentice, 1980). For WA-PLS modelling, tree-cover data were square-root transformed, and the number of components was selected using a randomization *t*-test (Juggins and Birks, 2012). The accuracy of the approach was evaluated for the modern data using leave-one-out cross-validation by comparing the AVHRR observations at each surface sample location to the percentage cover associated with the most similar modern analogues. The inherent "edge effect" of the unimodal-based method (e.g. WA-PLS) results in distortions at the end of environmental gradient (ter Braak and Juggins, 1993), particularly for large spatial-scale calibration-set (Birks, 1998), therefore, we only presented and discussed the results produced by MAT and included results from WA-PLS in the supplementary material (Appendix 3).

3.4. Forest cover from climate modelling

To evaluate the proxy-based results, reconstructions were compared to results from the application of the ECHAM5/JSBACH climate model (Dallmeyer et al., 2013). The model has a spectral resolution of T106L31, which corresponds to 1.125° in a Gaussian grid. The model consists of a general circulation model for the atmosphere ECHAM5 (Roeckner et al., 2003) coupled to the land-surface scheme JSBACH (Raddatz et al., 2007). We analysed the vegetation results of experiments representing three different time-slices, i.e. 9 ka BP (early Holocene), 6 ka BP (mid-Holocene), and 0 ka BP (pre-industrial). For all simulations, the atmospheric composition was kept constant at pre-industrial levels, for example, the CO_2-concentration was set to 280 ppm. JSBACH includes a dynamic vegetation module (Brovkin et al., 2009) that categorizes the vegetation into eight plant functional types (PFTs). Trees are distinguished as tropical or extratropical and are either deciduous or evergreen. Shrubs are differentiated between raingreen and cold shrubs and grass is separated into either C3 or C4 grass. The land surface in JSBACH is tiled in mosaics, thus, several PFTs can cover one grid-cell. The grid-cell is further divided into vegetated and non-vegetated areas, i.e. seasonally bare ground and desert. In this study, we aggregated the PFTs into woody vegetation (all trees and shrubs) and non-woody types.

For each PFT, environmental constraints (e.g. temperature threshold) are defined that represent the bioclimatic tolerance of the plants and determine the area where the different PFTs can establish. The fractional cover of each PFT is then determined by the balance of mortality (including disturbances such as windthrow, fire and natural ageing) and establishment. Establishment is calculated based on the relative differences in annual net primary productivity (NPP) of the PFTs whilst also considering the moisture requirements of the plants. Simulated vegetation changes can thus be caused by bioclimatic shifts (i.e. temperature changes), changes in the frequency of disturbance or changes in plant productivity. A detailed description of the handling of dynamic vegetation in the model is given in Brovkin et al. (2009), Dallmeyer et al. (2011) and

Dallmeyer and Claussen (2011).

4. Results

4.1. Assessment of the MAT models

The pollen-based modern woody cover estimations and original AVHRR measurements match well (Figs. 2 and 3; Appendix 2), with high r^2 (coefficient of determination between observed and predicted values) and low RMSEP (root mean squared error of prediction) for total tree, broadleaved and needleleaved cover, although the predicted estimates show slight trends of underestimation for high woody cover sites. For most sites the residuals between pollen-based modern woody cover estimations and AVHRR-based observations are between −5 and 5% and are mainly located in the areas with intermediate AVHRR-based cover, while some sites with greater than 25% or lower than −25% are located mainly in areas with relatively high total tree and needleleaved cover (Fig. 3). Broadleaved tree cover has the lowest residuals, whilst total tree cover has the highest residuals (Fig. 3).

4.2. Variations in forest cover since the last glacial maximum

Before the last deglaciation (22–16 ka BP), tree cover was lowest throughout the study area, and sites with relatively high tree cover are mainly located in tropical and subtropical areas (Fig. 4; Appendix 2). After 15 ka BP, tree cover across most of the study area started to increase with the most significant changes occurring during 12–9 ka BP. Total tree cover reached its maximum at around 8 ka BP. During the last deglaciation, increases in forest cover from 18 to 15 ka BP and 15–12 ka BP in the Asia monsoon boundary area were mainly caused by an increase in needleleaved cover, while broadleaved cover started to increase during 12–9 ka BP. In addition, total tree cover and its patterns of change vary among areas: the forest-steppe transition zone has the most notable variations over the last 22 kyr.

4.3. Regional differences in the temporal evolution of forest cover

To examine the patterns of tree-cover extent in different areas, we assigned our records to six sub-regions based on differences in vegetation type, topography and climate characteristics. Sub-region 1 is the rainforest and evergreen broadleaved forest in the south-eastern part of our study area and has the highest modern forest cover; sub-region 2 is the forest-steppe transition zone in north-central China; sub-region 3 is the north-eastern part of study area; sub-region 4 is the eastern rim of the Tibetan Plateau; sub-region 5 includes the present-day steppe and desert areas with the lowest modern forest cover; and sub-region 6 is the forest-steppe transition zone in the north-west of our study region including parts of northern Mongolia and southern Siberia (Fig. 1). Both sub-regions 1 and 5 show only minor changes in woody cover during the last 22 kyr, while the other four sub-regions show distinct temporal patterns in woody cover (Fig. 5; Appendix 2). For example, total tree cover in sub-region 2 increased strongly from 16 ka BP and reached a maximum during 8–5.5 ka BP, then decreased markedly, especially during the late Holocene (after 4 ka BP) when cover became less than 30%. Sub-region 3 had high localized total tree cover as recorded in a few pollen records from the Changbai Mountain and coastal area before the Holocene, which then spread broadly during the latter half of the Holocene (from 6.5 ka BP). In sub-region 4, total tree cover increased markedly around 14.5 ka BP and reached its spatial maximum during 13.5–9 ka BP, then decreased during the mid and late Holocene (since ca. 8 ka BP). Total tree cover started to increase after 15.5 ka BP in sub-region 6 and cover greater than 10% was restricted to northern Mongolia and southern Siberia. After ca. 11.5 ka BP, the area of high total tree cover occurred in western parts (Altai Mountains and adjacent areas to the west) and total tree cover reached its maximum spatial extent in the mid Holocene (after ca. 5.5 ka BP).

4.4. Simulated woody cover for 9, 6 and 0 ka BP

The spatial extent of the simulated woody cover for the three key time slices 9, 6 and 0 ka BP is rather similar (see maps of absolute cover in Appendix 4). However, forest cover changes are more pronounced in some areas (see maps of differences in forest cover for 9–6 and 6–0 ka BP in Fig. 6). The strongest temporal changes occur on the eastern margin of the Tibetan Plateau (sub-region 4) and, to a lesser extent, in the forest-steppe transition zones in north-central China (sub-region 2) with generally decreasing trends since 9 ka BP. In contrast, no notable changes (mostly between −5% and +5%) occur in the tropical and subtropical areas of south-eastern China (sub-region 1) and arid central Asia including the western Tibetan Plateau (sub-region 5). In north-eastern China (sub-region 3), changes are also small, although in areas north of 47°N an increase in total woody cover from 6 to 0 ka BP is a regionally widespread feature. While the lowland areas in the north-western region (sub-region 6) show no changes, the total tree cover decreases in the areas of the Mongolian Altai, the Sayan Mountains (Mongolia-Russia border area) and the Khentii Mountains in north-central Mongolia, particularly between 6 and 0 ka BP.

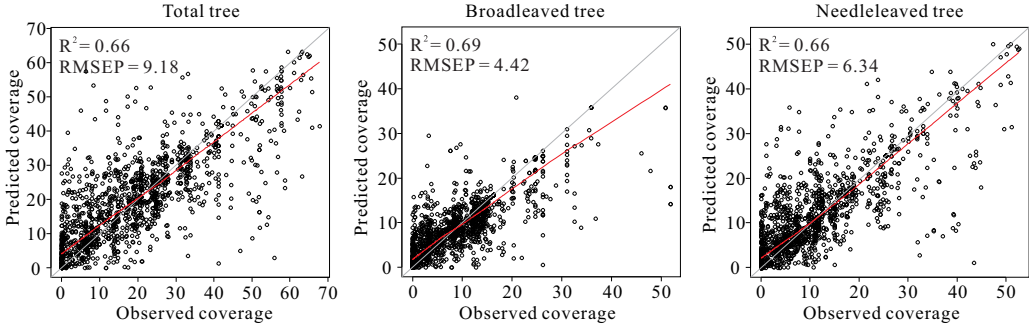

Fig. 2. Comparison of the AVHRR-derived observations of total tree, broadleaved, and needleleaved cover to the analogue-based percent cover estimates for modern pollen sites. R^2 is the coefficient of determination between observed and predicted tree cover and RMSEP is the root mean square error of prediction produced by the "leave-one-out" cross-validation.

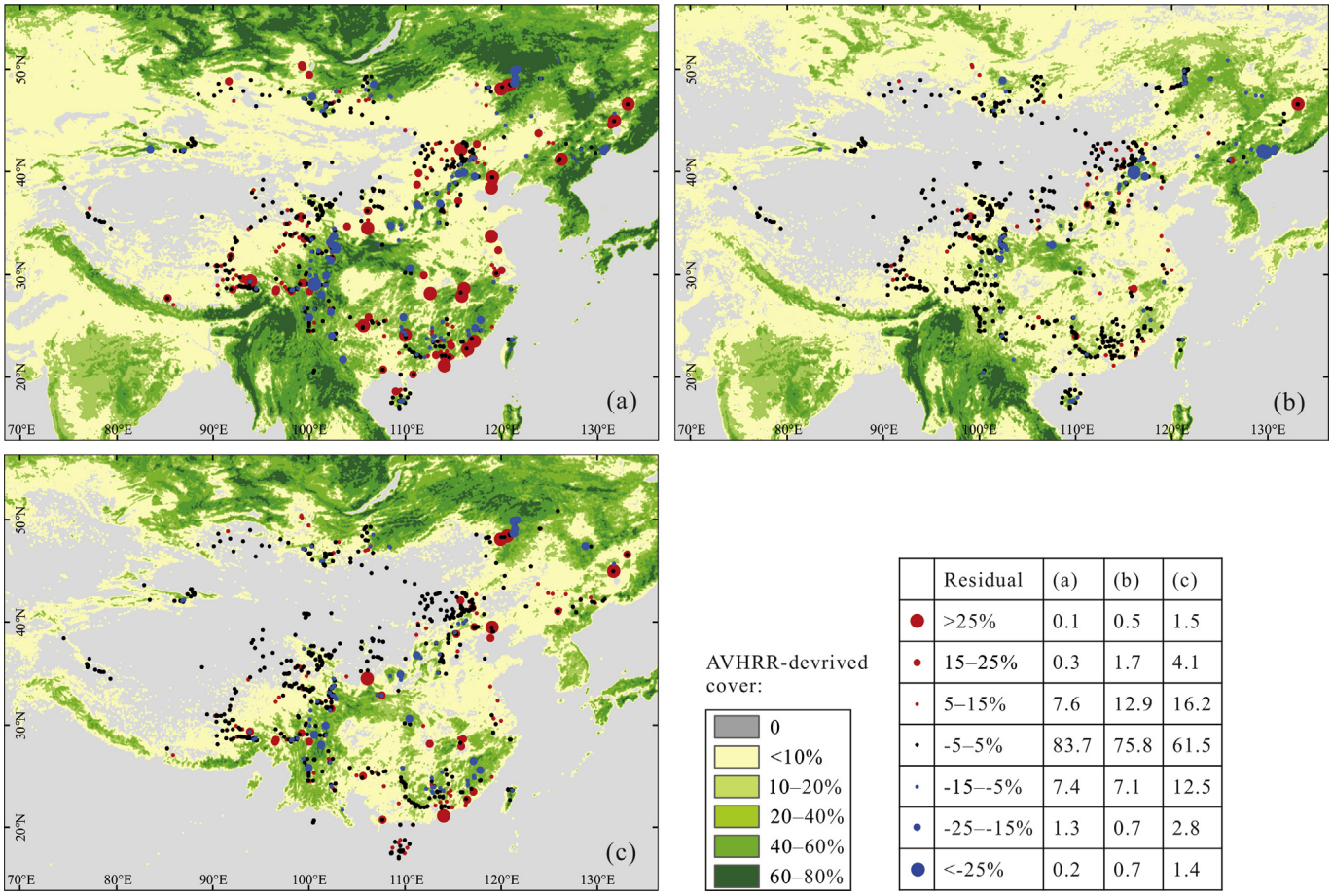

	Residual	(a)	(b)	(c)
●	>25%	0.1	0.5	1.5
●	15–25%	0.3	1.7	4.1
●	5–15%	7.6	12.9	16.2
●	-5–5%	83.7	75.8	61.5
●	-15–-5%	7.4	7.1	12.5
●	-25–-15%	1.3	0.7	2.8
●	<-25%	0.2	0.7	1.4

Fig. 3. The residuals between pollen-based reconstructions and AVHRR-derived observations for all the modern pollen sites: (a) total tree cover (the total tree cover for grids with values lower than 10% are set to 1% in the background map, but for all analyses we calculated them as the sum of broadleaved and needleleaved cover), (b) broadleaved cover, (c) needleleaved cover. The numbers in the table in the lower right of the figure show the proportion of modern pollen sites available within different ranges of residuals between pollen-based reconstructions and AVHRR-derived observations (reconstruction minus observation).

5. Discussion

5.1. Evaluation of the quality of the calibration and the reliability of reconstructions

Comparison of the AVHRR data to other remotely sensed land-cover datasets suggests a good agreement (69–84%) in percent total tree cover, but AVHRR predicts somewhat higher values for sparsely wooded locations (DeFries et al., 2000). Past tree cover reconstructions based on AVHRR data might, therefore, over-estimate cover in areas of low tree cover. Furthermore, modern pollen assemblages generally represent a multi-year vegetation signal, and thus a multi-year mean of tree cover would be more suitable for comparison. More than the half of our modern pollen data were collected between 1964 and 1999 (Cao et al., 2014), which means that they integrate a multiyear signal which is certainly before the start of the most recently published multi-year tree cover database (2000–2013) of Hansen et al. (2013). Accordingly we used the older AVHRR dataset (using images from 1990 to 1993) which, in addition also allows a better comparability with reconstruction by Tarasov et al. (2007) for northern Asian that are based on the same remote sensing product. Nevertheless, in a pollen-based tree cover reconstruction, the spatial mean of tree cover could, to some extent, offset the effect of the temporal mismatch between tree cover and pollen data.

Our coefficients of determination (r^2) between observed and predicted forest cover values based on MAT are of a similar magnitude of those for North America and northern Eurasia (r^2 of needleleaved cover 0.66 and 0.79 and r^2 of broadleaved cover 0.86 and 0.66, respectively, vs 0.66 and 0.69 for our results; Williams, 2003; Williams and Jackson, 2003; Tarasov et al., 2007). Our r^2 for total tree cover (0.66) is also similar to that of Zheng et al. (2010; 0.69; see Figs. 2 and 3, Appendix 2). Our study also tests, for the first time, the spatial autocorrelation effect in a pollen-forest cover calibration-set. We find that both numerical methods applied (MAT and WA-PLS) are potentially influenced by spatial autocorrelation, particularly MAT. The model performances for the two methods, indicated by r^2 values, reduces sharply when sites within a 20 km radius are deleted from cross-validation, implying that these neighbourhood sites play an important role in improving model performances. Beyond the 20 km neighbourhood, r^2 values are ~0.3 for both methods (Appendices 2 and 3), indicating that the pollen-based modern woody cover reconstructions and the original AVHRR-derived vegetation data match well generally. Some individual samples, however, show high residuals that may originate from the heterogeneity of the sedimentary origin of the modern pollen data even though we excluded samples from very large lakes so as to be representative of local vegetation (Sugita, 1993; Jackson and Kearsley, 1998). The included sample types (surface soil, small lakes, moss polster) have pollen source areas of varying extent and may thus affect the pollen-vegetation relationship. In addition, the difference between pollen source area and half-width of the search

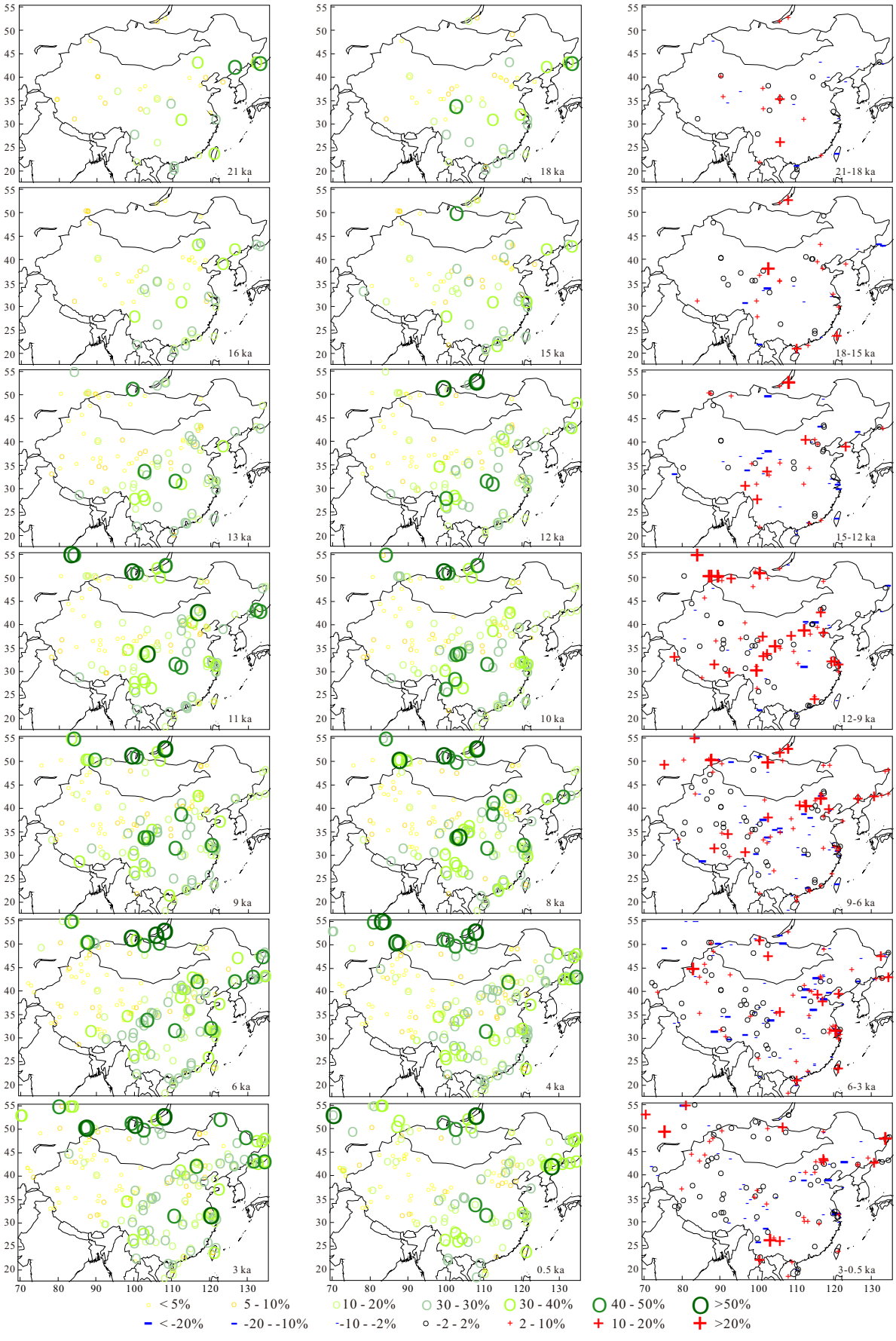
21 ka
18 ka
21-18 ka
16 ka
15 ka
18-15 ka
13 ka
12 ka
15-12 ka
11 ka
10 ka
12-9 ka
9 ka
8 ka
9-6 ka
6 ka
4 ka
6-3 ka
3 ka
0.5 ka
3-0.5 ka
< 5%
5 - 10%
10 - 20%
30 - 30%
30 - 40%
40 - 50%
>50%
< -20%
-20 - -10%
-10 - -2%
-2 - 2%
2 - 10%
10 - 20%
>20%

window for extracting tree-cover data would give rise to errors in the interpretation of palynological data too.

Many modern pollen samples were collected from the patchy forest in the eastern and southern parts of the study area, which have been intensively used for agriculture; less-disturbed forest only occurs in hilly and mountainous areas. These pollen assemblages would be affected by the local arboreal pollen type. Search window half-widths of between 25 and 100 km are recommended for AVHRR estimates (Williams and Jackson, 2003), but forest cover could be overestimated and cause positive residuals when too large a window size is selected. Conversely, for samples collected from farmland surrounded by forest, a small window size could cause underestimation of forest cover and produce negative residuals. In order to reconcile best these issues, we chose a moderate search window size of 50 km half-width, which is approximately the transportation distance for common arboreal taxa pollen (e.g. Zhu et al., 2003). Nevertheless, a 50 km search window might be too large for the patchy forest in our south-eastern areas and cause exaggerated residuals (Fig. 3). The mismatch in spatial scale between the relevant source area of the pollen records and the 50 × 50 km search window of the AVHRR data could thus cause both underestimation and overestimation of tree cover. For example, in the low tree-cover areas of the western part in the study area, the long-distant transport of arboreal pollen from forested areas would influence the composition of pollen spectra substantially, and would result in the overestimation of tree cover.

Williams (2003) points out that the underestimated woody cover in Alaska in North America may be caused by the relatively sparse number of modern pollen samples, while higher estimates for central North America are related to the identification of analogues from regions less affected by human land-use. Our modern pollen samples cover all the major vegetation types of the study area, providing the opportunity to find the closest analogue for the fossil records. Still large-scale human impact as well as changes in the atmospheric CO_2 concentration may reduce the analogue quality for the late-glacial and early-Holocene samples.

An uneven distribution of samples along environmental gradients can bias the RMSEP (Telford and Birks, 2011). In our case, the relatively low number of samples from forest with high woody cover could cause high residuals in the reconstructions, especially for broadleaved cover, as well as affecting reconstructions in the eastern part of the study area (Figs. 2 and 3). Such discrepancies were also found in studies for northern Eurasia and North America, which both underestimated woody cover in high tree cover areas (particularly in patchy forest areas), and overestimated tree density for sparsely wooded locations (Williams, 2003; Tarasov et al., 2007).

5.2. Woody cover changes over the last 22 kyr

Overall, the reconstructions reveal a long-term increase in forest cover from the Last Glacial Maximum to the mid Holocene. The woody cover reconstructions suggest that the low tree cover during the LGM occurred throughout the whole study area, which agrees well with qualitative interpretations of the original pollen records and with regional vegetation reconstructions (Tarasov et al., 2000; Herzschuh et al., 2010; Liu et al., 2013; Ni et al., 2010; 2014). Forest cover developed during the early Holocene and flourished in the early mid-Holocene. A gradual decrease of forest cover occurred in parts of the study area during the late Holocene (e.g. Ren, 2007).

Our pollen-based forest-cover reconstruction agrees with most reconstructions of the original pollen data: it does not show a large-scale change in forest spatial extent over the last 22 kyr, but does indicate marked forest-cover changes on a regional to local scale, particularly in the forest-steppe transition areas, consistent with previous regional studies (north-central China, sub-region 2; Xiao et al., 2004; Sun et al., 2006; Liu et al., 2013; the eastern margin of the Tibetan Plateau, sub-region 4: Shen et al., 2005; Kramer et al., 2010a, 2010b; Herzschuh et al., 2014; and north Mongolia and south Siberia, sub-region 6: Bezrukova et al., 2010; Tian et al., 2014).

The model-simulated woody cover during the Holocene is of stable spatial extent for forest, which is generally consistent with the modern forest range and our pollen-based reconstruction. Simulated total tree-cover also indicates that the marked changes are restricted to the forest-steppe transition areas and have a similar temporal change pattern (general decrease) to the pollen-based quantitative reconstruction for the Holocene. In sub-regions 2 and 4, the relative changes in tree cover from 9 to 0 ka BP generally match well between pollen-inferred reconstructions and modelled estimations. For example, in sub-region 2, the changes range between 5% and 10% under both approaches, and in sub-region 4, the relative changes are about 15% in the pollen-based reconstruction and 20% or less in the modelling approach. However, the absolute forest cover of the pollen-based reconstruction is generally lower for those areas where cover is less than 30% (Fig. 5), whilst the modelled reconstruction is mostly higher (Appendix 4). This finding highlights three shortcomings of the pollen-based approach. First, pollen samples from areas with high forest cover are underrepresented in the calibration set – only 24% of available modern pollen sites have >30% tree cover. Second, modern forest from eastern China is impacted by human activities, and even though sites with more natural vegetation were preferred for sampling of modern pollen, the regional pollen load will have originated from patchy vegetation. Third, differences in the forest reconstruction arise from the fact that the modelled vegetation does not consider human impact on vegetation. In summary, the pollen-inferred tree-cover reconstruction may underestimate forest cover, but relative change ranges can be considered as reasonable.

5.3. The major driver of woody cover changes

In the study area, annual precipitation is considered as the most important determinant of the spatial vegetation distribution (Hou, 1983; Fang et al., 2005), and vegetation has been observed to respond sensitively to precipitation change on decadal time-scales (Poulter et al., 2013). In addition, precipitation best explains modern pollen assemblages from the eastern continental area while temperature-related variables are subordinate (Cao et al., 2014). Therefore, vegetation change on a millennial time-scale is expected to reflect mainly precipitation changes, but the relative importance of the climate variables for vegetation change may have changed through time (Stebich et al., 2015).

Low tree-cover density in the LGM in our study area is likely caused by a combination of colder-than-present temperatures, lower-than-present precipitation levels, and lower-than-present atmospheric CO_2 concentrations. A weak East Asian Summer Monsoon during the LGM is indicated by many speleothem records from southern China (e.g. Yuan et al., 2004; Wang et al., 2005). Glacier records and climate simulations suggest that the LGM was much drier and colder on the Tibetan Plateau and even in the whole of China (Shi et al., 1997; Jiang et al., 2011). A cold and dry LGM is

Fig. 4. Total tree cover reconstructions for key time-slices (first two columns) with temporal changes at 3-kyr intervals (last column) over the last 22 kyr.

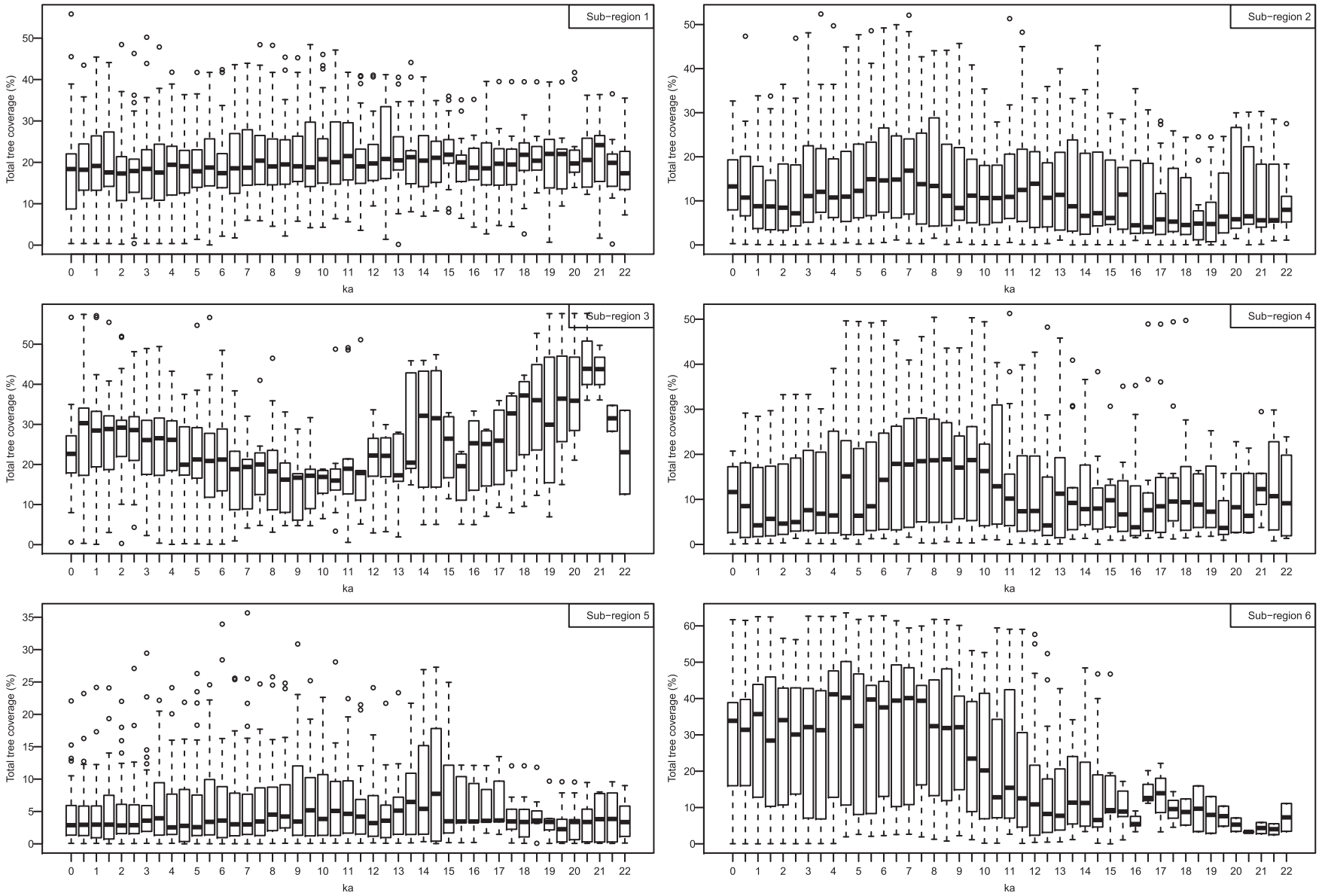

Fig. 5. Patterns of total tree cover in the six sub-regions over the last 22 kyr. Sub-region 1, south-eastern China; Sub-region 2, north-central China; Sub-region 3, north-eastern China and Russia Far East; Sub-region 4, eastern Tibetan Plateau; Sub-region 5, arid central Asia; and Sub-region 6, northern Mongolia and southern Siberia.

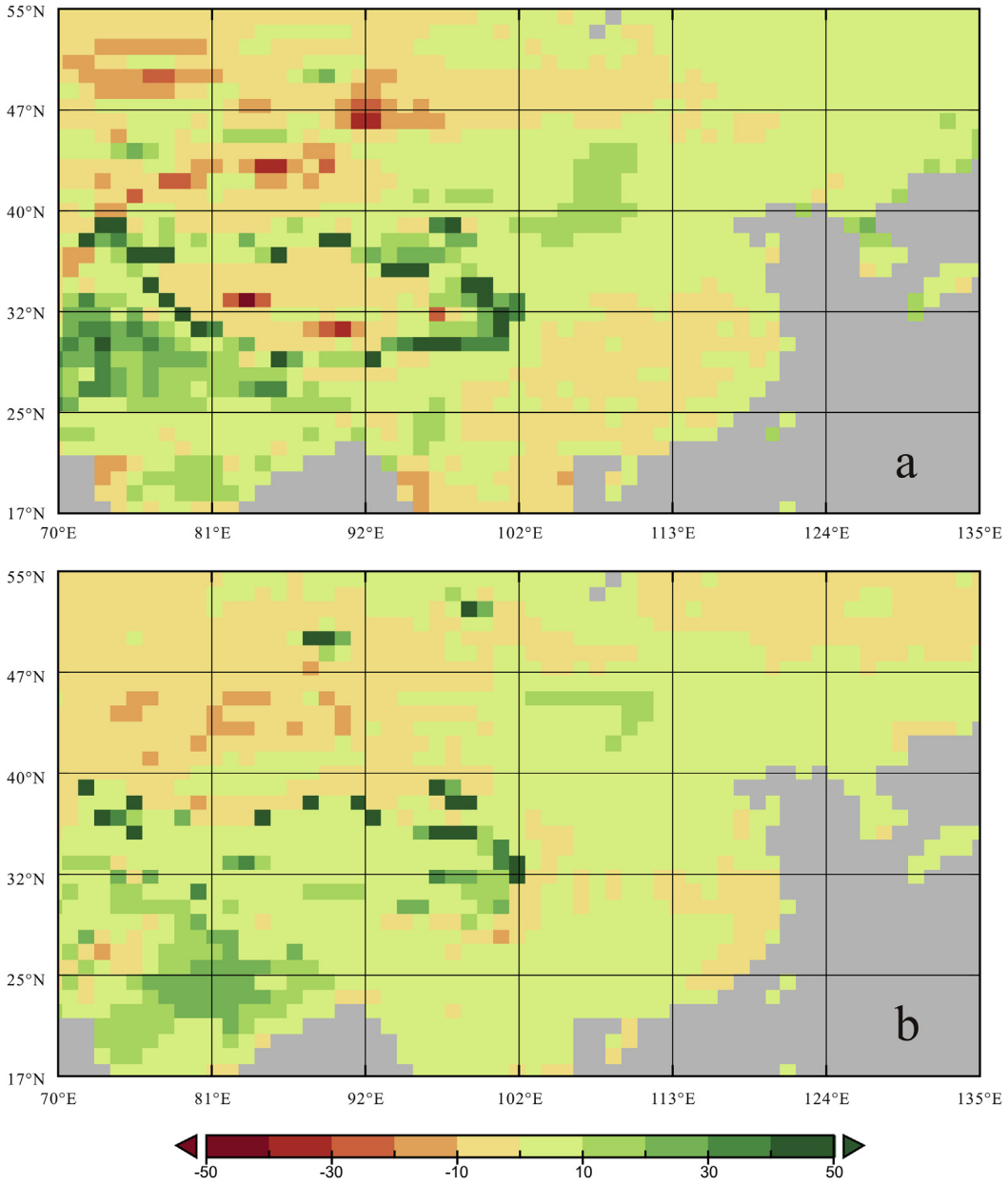

Fig. 6. Modelled difference in total woody cover for (a) between 9 and 6 ka BP and (b) between 6 and 0 ka BP (woody cover at older time slices minus that at younger time slices).

also inferred for northern Mongolia and southern Siberia (e.g. Fedotov et al., 2004). The low temperatures, but particularly the dry climate and the low atmospheric CO_2 in the LGM, are possible reasons for the restricted forest distribution, particularly in forest-steppe transition areas, which are sensitive to climate change (Levis et al., 1999; Herzschuh et al., 2011). Climate simulations suggest suitable climatic conditions for forest growth (annual surface temperatures of ca. 11–16 °C and annual precipitation of >900 mm) were found during the LGM in the present tropical and subtropical areas (sub-region 1) (Ju et al., 2007; Jiang et al., 2011), which may have allowed the steady high woody cover since the LGM in that region (Fig. 5; Appendix 2). In contrast, the arid central Asian region (sub-region 5) never received sufficient moisture for forest development during the last 22 kyr, not even during the mid-Holocene optimum, and forest cover consequently stayed low and stable there. The East Asian Summer Monsoon was strongest at the beginning of the Bølling/Allerød (B/A; ca. 14.5 ka BP) and Holocene (ca. 11.5 ka BP) (Yuan et al., 2004; Wang et al., 2005), causing high precipitation rates (Herzschuh, 2006; Wang et al., 2010) and is reflected by the high reconstructed forest cover (particularly in sub-regions 2, 4 and 6). Synthesis studies for the first half of the Holocene using non-pollen palaeoclimate proxy records (Wang et al., 2010) or lake-level reconstructions (Li and Morrill, 2010), also reveal that high precipitation (or moisture) occurs in monsoonal East Asia, explaining the higher reconstructed forest cover in the monsoon fringe areas (sub-regions 2 and 4).

Because the trends of the modelled forest cover changes resemble those of the reconstructions, the modelled climate changes can be used to explore the driving mechanism of forest-cover changes. The results of the climate model reveal a decrease in total annual precipitation from 9 to 6 and 6 to 0 ka BP, which is likely to be the major driving factor for the decreasing forest cover. At the higher elevation of the eastern Tibetan Plateau margin, a cooler summer climate (resulting in GDD <350°) is an additional

bioclimatic parameter that could have hindered forest development at 6 ka BP and 0 ka BP compared to 9 ka BP.

Since the late Holocene (after ca. 4 ka BP), annual surface temperature decreased throughout the study region (Wang et al., 2010; Yu, 2013), but annual precipitation had different patterns in the different regions. In north-central China (sub-region 2) and the north-eastern margin of the Tibetan Plateau (sub-region 4), the weaker monsoon intensity during the late Holocene reduced annual precipitation (Liu et al., 2014), which could explain the gradual decrease of forest cover in the forest-steppe transition areas. Early agriculture was widespread in the eastern part of the study area during the late Holocene, and deforestation occurred, particularly on the eastern plains (Fu, 2003; Gong et al., 2003, 2007; Li et al., 2009; Lu et al., 2009). Many previous studies thus consider that the decline in forest cover during the late Holocene may have been caused predominantly by human activities (e.g. Zheng et al., 2004; Ren, 2007; Cao et al., 2010). Our late-Holocene forest-cover reconstruction trends correlate well with the modelling results for 6–0 ka BP, so it is plausible to argue that natural causes contributed markedly to the forest decline in continental eastern Asia on a continental scale. Human impact still has important effects on the vegetation at a regional scale, for example, the relatively remarkable tree-cover changes for special sites from the south-eastern part of China. In addition, the deteriorating climate of the late Holocene might amplify the effects of human impact or vice versa. Particularly in north-central China, an unfavourable climate generated vulnerable vegetation, which is easily disturbed by human activities and the restoration of the natural vegetation would be difficult under poor climate conditions. Similar complex interactions are proposed for recent vegetation change in arid China (Wang et al., 2004).

5.4. Comparison of tree-cover patterns across continents

The general temporal pattern of woody cover with a relatively low forest cover in the glacial period and higher forest cover in the interglacial period is similar for eastern continental Asia, northern Eurasia (Tarasov et al., 2007) and North America (Williams, 2003). However, there also occur marked differences, even between northern Eurasia and our study in East Asia.

(1) Spatial extent of forest: there have been significant changes in the distribution of forest across North America since the LGM, with a marked northward spread (Williams, 2003). Binney et al. (2009) confirm that boreal forest taxa (*Larix*, *Picea*, *Pinus, Abies*) significantly migrated northward in northern Eurasia during the last glacial-interglacial cycle based on plant macrofossils. However, in our study, the modern forest distribution is not very different from that of the LGM and tree taxa migration played a minor role (Cao et al., 2015). In North America, a study on continental-scale relationships between modern pollen and climate, suggests that temperature is the most important climatic determinant of pollen distribution (Williams and Shuman, 2008). There is no similar study in northern Eurasia, although a regional study on modern pollen (Klemm et al., 2013) and some continental-scale past biome (vegetation) reconstructions (Prentice et al., 1992; Tarasov et al., 2007) suggest that temperature is more important than precipitation in determinating plant distribution. During the LGM, the estimated annual surface temperature on the two continents were 10–20 °C colder than present (Kageyama et al., 2001; Marshall et al., 2002), which could seriously restrict forest distribution. Forest expanded northwards in the subsequent interglacial period. In monsoonal East Asia, precipitation plays a more important role in forest distribution than in North America and northern Eurasia (Fang et al., 1996; Poulter et al., 2013), as supported by the continental-scale relationship between modern pollen and climate found by Cao et al. (2014). The estimated annual surface temperature was only lower than present-day (~2–7 °C) in China in the LGM (Jiang et al., 2011), hence forest could survive during the LGM in habitats with suitable effective moisture, which are found from south to north at lower elevations in eastern areas. On the Tibetan Plateau, glacial forest refugia were restricted to lower elevation areas until the climate started to warm up at the beginning of the Holocene (Herzschuh et al., 2014), while the moisture increase during the Bølling/Allerød did not strongly affect the woody cover. In contrast, the presence of a continental-scale glacier during the LGM in North America and northern Eurasia (Peltier and Fairbanks, 2006) restricted forest distribution, with trees and forest spreading northwards only after glacier retreats (Jackson et al., 1997; Williams, 2003; Feurdean et al., 2013). In our study region, the lack of a continental glacier during the LGM (Shi, 2005) could explain the relatively warm LGM compared to Europe and North America (Svendsen et al., 2004) and permit the broader distribution of forest.

(2) Strength of human impact: forest cover reduced markedly in the monsoon fringe areas during the late Holocene. This could be due to a weaker summer monsoon, although it is a time of enhanced human impact that may have reduced forest cover directly, as well as causing soil erosion and reducing effective moisture, thereby negatively affecting forest cover indirectly (e.g. Makohonienko et al., 2004; He et al., 2006). In south-eastern China, although forest cover had no notable decrease at a large spatial scale during the late Holocene, human impacts (Li et al., 2009) likely reduced forest cover at a local scale. In North America, needleleaved and broadleaved tree densities continued to increase during the Holocene until widespread European settlement (ca. 200 years ago), which generally reflects the relatively stable climate (Williams, 2003). In northern Asia, no noticeable forest-cover changes were detected by the four pollen records, and human impact was not considered as a major influence (Tarasov et al., 2007). The low-level and short-term human impact histories in North America and northern Asia imply that forest cover until the 18th century, in contrast to eastern Asia, is almost exclusively controlled by climate change.

6. Conclusions

The modern pollen dataset from China and Mongolia correlates well with the AVHRR-derived vegetation data, and a test with the modern analogue technique shows it can reproduce present-day characteristics of woody cover in eastern continental Asia well, although relatively high residuals occur in some areas with high cover. Our pollen-based woody cover reconstructions indicate significant woody cover changes in eastern continental Asia since 22 ka BP, especially at the eastern margin of the Tibetan Plateau and in the forest-steppe transition areas in north-central China, but the overall spatial forest extent did not change markedly at the continental scale. The Holocene decrease in woody cover from forest-steppe transition areas is related to the weakening of the moisture delivered by the Asian Summer Monsoon and, in mountainous areas, also by the decline of summer temperature. The general glacial-declacial trend (low-to-high forest cover) is similar for eastern continental Asia, North America and northern Eurasia (from where similar datasets are available). The Holocene history in

eastern continental Asia is unique because of its strong precipitation-driven nature and long-term human impact.

Acknowledgements

This study was supported by the German Research Foundation (DFG) and the National Natural Science Foundation of China (NSFC). The doctoral research of Fang Tian and Xianyong Cao were funded by the "Helmholtz–China Scholarship Council (CSC) Young Scientist Fellowship" (No. 20100813030; 20100813031). Yan Zhao was supported by NSFC (No. 41330105).

Appendix A. Supplementary data

Supplementary data related to this article can be found at http://dx.doi.org/10.1016/j.quascirev.2016.02.001.

References

Bezrukova, E.V., Tarasov, P.E., Solocieva, N., Krivonogov, S.K., Riedel, F., 2010. Last glacial–interglacial vegetation and environmental dynamics in southern Siberia: chronology, forcing and feedbacks. Palaeogeogr. Palaeoclimatol. Palaeoecol. 296, 185–198.

Binney, H.A., Willis, K.J., Edwards, M.E., Bhagwat, S.A., Anderson, P.M., Andreev, A.A., Blaauw, M., Damblon, F., Haesaerts, P., Kienast, F., Kremenetski, K.V., Krivonogov, S.K., Lozhkin, A.V., MacDonald, G.M., Novenko, E.Y., Oksanen, P., Sapelko, T.V., Väliranta, M., Vazhenina, L., 2009. The distribution of late-quaternary woody taxa in northern Eurasia: evidence from a new macrofossil database. Quat. Sci. Rev. 28, 2445–2464.

Birks, H.J.B., 1998. Numerical tools in palaeolimnology–progress, potentialities, and problems. J. Paleolimnol. 20, 307–332.

Bradshaw, R.H.W., Webb III, T., 1985. Relationships between contemporary pollen and vegetation data from Wisconsin and Michigan, USA. Ecology 66, 721–737.

Brovkin, V., Raddatz, T., Reick, C.H., Claussen, M., Gayler, V., 2009. Global biogeophysical interactions between forest and climate. Geophys. Res. Lett. 36, L07405. http://dx.doi.org/10.1029/2009GL037543.

Campo, E.V., Gasse, F., 1993. Pollen- and diatom-inferred climatic and hydrological changes in Sumxi Co Basin (Western Tibet) since 13,000 yr B.P. Quat. Res. 39, 300–313.

Cao, X., Xu, Q., Jing, Z., Li, Y., Tian, F., 2010. Holocene climate change and human impacts implied from the pollen records in Anyang, central China. Quat. Int. 227, 3–9.

Cao, X.Y., Herzschuh, U., Ni, J., Zhao, Y., Böhmer, T., 2015. Spatial and temporal distributions of major tree taxa in eastern continental Asia during the last 22,000 years. Holocene 25, 79–91.

Cao, X.Y., Herzschuh, U., Telford, R.J., Ni, J., 2014. A modern pollen-climate dataset from China and Mongolia: assessing its potential for climate reconstruction. Rev. Palaeobot. Palynol. 211, 87–96.

Cao, X.Y., Ni, J., Herzschuh, U., Wang, Y.B., Zhao, Y., 2013. A late Quaternary pollen dataset in eastern continental Asia for vegetation and climate reconstructions: set-up and evaluation. Rev. Palaeobot. Palynol. 194, 21–37.

Dallmeyer, A., Claussen, M., 2011. The influence of land cover change in the Asian monsoon region on present-day and mid-Holocene climate. Biogeosciences 8, 1499–1519.

Dallmeyer, A., Claussen, M., Herzschuh, U., Fischer, N., 2011. Holocene vegetation and biomass changes on the Tibetan Plateau: a model-pollen data comparison. Clim. Past 7, 881–901.

Dallmeyer, A., Claussen, M., Wang, Y., Herzschuh, U., 2013. Spatial variability of Holocene changes in the annual precipitation pattern – a model-data synthesis for the Asian monsoon region. Clim. Dyn. 40, 2919–2936.

DeFries, R.S., Hansen, M.C., Townshend, J.R.G., Janetos, A.C., Loveland, T.R., 2000. 1 Kilometer Tree Cover Continuous Fields, 1.0. Department of Geography, University of Maryland, College Park, Maryland, pp. 1992–1993.

DeFries, R.S., Townshend, J.R.G., Hansen, M.C., 1999. Continuous fields of vegetation characteristics at the global scale at 1-km resolution. J. Geophys. Res. Atmos. 104, 16911–16923.

Fang, J.Y., Ohsawa, M., Hira, T., 1996. Vertical vegetation zones along 30°N latitude in humid East Asia. Plant Ecol. 126, 135–149.

Fang, J.Y., Piao, S.L., Zhou, L.M., He, J.S., Wei, F.Y., Myneni, R.B., Tucker, C.J., Tan, K., 2005. Precipitation patterns alter growth of temperature vegetation. Geophys. Res. Lett. 32, 411–415.

Fedotov, A.P., Chebykin, E.P., Yu, S.M., Vorobyova, S.S., Yu, O.E., Golobokova, L.P., Pogodaeva, T.V., Zheleznyakova, T.O., Grachev, M.A., Tomurhuu, D., Oyunchimeg, T., Narantsetseg, T., Tomurtogoo, O., Dolgikh, P.T., Arsenyuk, M.I., Batist, M.D., 2004. Changes in the volume and salinity of Lake Khubsugul (Mongolia) in response to global climate changes in the upper Pleistocene and the Holocene. Palaeogeogr. Palaeoclimatol. Palaeoecol. 209, 245–257.

Feurdean, A., Bhagwat, S.A., Willis, K.J., Birks, H.J.B., Lischke, H., Hickler, T., 2013. Tree migration-rates: narrowing the gap between inferred post-glacial rates and projected rates. PLoS One 8, e71797.

Fu, C., 2003. Potential impacts of human-induced land cover change on East Asia monsoon. Glob. Planet. Change 37, 219–229.

Gong, Z., Zhang, X., Chen, J., Zhang, G., 2003. Origin and development of soil science in ancient China. Geoderma 115, 3–13.

Gong, Z.T., Chen, H.Z., Yuan, D.G., Zhao, Y.G., Wu, Y.J., Zhang, G.L., 2007. The temporal and spatial distribution of ancient rice in China and its implications. Chin. Sci. Bull. 52, 1071–1079.

Hansen, M.C., Potapov, P.V., Moore, R., Hancher, M., Turubanova, S.A., Tyukavina, A., Thau, D., Stehman, S.V., Goetz, S.J., Loveland, T.R., Kommareddy, A., Egorov, A., Chini, L., Justice, C.O., Townshend, J.R.G., 2013. High-resolution global maps of 21st-century forest cover change. Science 342, 850–853.

He, X., Zhou, J., Zhang, X., Tang, K., 2006. Soil erosion response to climatic change and human activity during the Quaternary on the Loess Plateau, China. Reg. Environ. Change 6, 62–70.

Herzschuh, U., 2006. Palaeo-moisture evolution in monsoonal Central Asia during the last 50,000 years. Quat. Sci. Rev. 25, 163–178.

Herzschuh, U., Birks, H.J.B., Ni, J., Zhao, Y., Liu, H., Liu, X., Grosse, G., 2010. Holocene land-cover changes on the Tibetan Plateau. Holocene 20, 91–104.

Herzschuh, U., Borkowski, J., Schewe, J., Mischke, S., Tian, F., 2014. Moisture-advection feedback supports strong early-to-mid Holocene monsoon climate on the eastern Tibetan Plateau as inferred from a pollen-based reconstruction. Palaeogeogr. Palaeoclimatol. Palaeoecol. 402, 44–54.

Herzschuh, U., Ni, J., Birks, H.J.B., Böhner, J., 2011. Driving forces of mid-Holocene vegetation shifts on the upper Tibetan Plateau, with emphasis on changes in atmospheric CO_2 concentrations. Quat. Sci. Rev. 30, 1907–1917.

Hou, H.Y., 1983. Vegetation of China with reference to its geographical distribution. Ann. Mo. Bot. Gard. 70, 509–549.

Jackson, S.T., 1990. Pollen source area and representation in small lakes of the northeastern United States. Rev. Palaeobot. Palynol. 63, 53–76.

Jackson, S.T., Kearsley, J.B., 1998. Quantitative representation of local forest composition in forest-floor pollen assemblages. J. Ecol. 86, 474–490.

Jackson, S.T., Overpeck, J.T., Webb III, T., Keattch, S.E., Anderson, K.H., 1997. Mapped plant-macrofossil and pollen records of late quaternary vegetation change in eastern North America. Quat. Sci. Rev. 16, 1–70.

Jiang, D., Lang, X., Tian, Z., Guo, D., 2011. Last glacial maximum climate over China from PMIP simulations. Palaeogeogr. Palaeoclimatol. Palaeoecol. 309, 347–357.

Ju, L., Wang, H., Jiang, D., 2007. Simulation of the last glacial maximum climate over East Asia with a regional climate model nested in a general circulation model. Palaeogeogr. Palaeoclimatol. Palaeoecol. 248, 376–390.

Juggins, S., 2012. Rioja: Analysis of Quaternary Science Data. Version 0.7–3. Available at: http://cran.r-project.org/web/packages/rioja/index.html.

Juggins, S., Birks, H.J.B., 2012. Quantitative environmental reconstructions from biological data. In: Birks, H.J.B., Lotter, A.F., Juggins, S., Smol, J.P. (Eds.), Tracking Environmental Change Using Lake Sediments, Data Handling and Numerical Techniques, vol. 5. Springer, Dordrecht, pp. 431–494.

Kageyama, M., Peyron, O., Pinot, S., Tarasov, P., Guiot, J., Joussaume, S., Ramstein, G., 2001. The last glacial maximum climate over Europe and western Siberia: a PMIP comparison between models and data. Clim. Dyn. 17, 23–43.

Klemm, J., Herzschuh, U., Pisaric, M., Heim, B., Telford, R., Pestryakova, L., 2013. Assessment of a modern pollen-climate calibration set for Arctic tundra and northern taiga biomes from northern Yakutia (Eastern Siberia) and its applicability to a Holocene record. Palaeogeogr. Palaeoclimatol. Palaeoecol. 386, 702–713.

Kramer, A., Herzschuh, U., Mischke, S., Zhang, C., 2010a. Late Quaternary environmental history of the south-eastern Tibetan Plateau inferred from the Lake Naleng non-pollen palynomorph record. Veg. Hist. Archaeobot. 19, 453–468.

Kramer, A., Herzschuh, U., Mischke, S., Zhang, C., 2010b. Holocene treeline shifts and monsoon variability in the Hengduan Mountains (Southeastern Tibetan Plateau), implications from palynological investigations. Palaeogeogr. Palaeoclimatol. Palaeoecol. 286, 23–41.

Krengel, M., 2000. Discourse on history of vegetation and climate in Mongolia-palynological report of sediment core Bayan Nuur I (NW-Mongolia). In: Walther, M., Janzen, J., Riedel, F., Keupp, H. (Eds.), State and Dynamics of Geosciences and Human Geography in Mongolia: Extended Abstracts of the International Symposium, Berliner Geowissenschaftliche Abhandlungen, pp. 80–84. Berlin, Germany.

Levis, S., Foley, J.A., Pollard, D., 1999. CO_2, climate, and vegetation feedbacks at the last glacial maximum. J. Geophys. Res. 104, 31191–31198.

Li, X., Dodson, J., Zhou, J., Zhou, X., 2009. Increases of population and expansion of rice agriculture in Asia, and anthropogenic methane emissions since 5000 BP. Quat. Int. 202, 41–50.

Li, Y., Morrill, C., 2010. Multiple factors causing Holocene lake-level change in monsoonal and arid central Asia as identified by model experiments. Clim. Dyn. 35, 1119–1132.

Liu, G., Yin, Y., Liu, H., Hao, Q., 2013. Quantifying regional vegetation cover variability in North China during the Holocene: implications for climate feedback. PLoS One 8 (8), e71681. http://dx.doi.org/10.1371/journal.pone.0071681.

Liu, M., Tian, H., 2010. China's land cover and land use change from 1700 to 2005: estimations from high-resolution satellite data and historical archives. Glob. Biogeochem. Cycles 24, GB3003. http://dx.doi.org/10.1029/2009GB003687.

Liu, Z., Wen, X., Brady, E.C., Otto-Bliesner, B., Yu, G., Lu, H., Cheng, H., Wang, Y., Zheng, W., Ding, Y., Edwards, R.L., Cheng, J., Liu, W., Yang, H., 2014. Chinese cave records and the East Asia summer monsoon. Quat. Sci. Rev. 83, 115–128.

Lu, H., Zhang, J., Liu, K.-B., Wu, N., Li, Y., Zhou, K., Ye, M., Zhang, T., Zhang, H., Yang, X.,

Shen, L., Xu, D., Li, Q., 2009. Earliest domestication of common millet (*Panicum miliaceum*) in East Asia extended to 10,000 years ago. Proc. Natl. Acad. Sci. U. S. A. 106, 7367–7372.
Makohonienko, M., Kitagawa, H., Naruse, T., Nasu, H., Monohara, A., Okuno, M., Fujiki, T., Liu, X., Yasuda, Y., Yin, H., 2004. Late-Holocene natural and anthropogenic vegetation changes in the Dongbei Pingyuan (Manchurian Plain), northeastern China. Quat. Int. 123–125, 71–88.
Marshall, S., James, T.S., Clarke, G.C., 2002. North American ice sheet reconstructions at the last glacial maximum. Quat. Sci. Rev. 21, 175–192.
Ni, J., Cao, X.Y., Jeltsch, F., Herzschuh, U., 2014. Biome distribution over the last 22,000 yr in China. Palaeogeogr. Palaeoclimatol. Palaeoecol. 409, 33–47.
Ni, J., Yu, G., Harrison, S.P., Prentice, I.C., 2010. Palaeovegetation in China during the late quaternary: biome reconstructions based on a global scheme of plant functional types. Palaeogeogr. Palaeoclimatol. Palaeoecol. 289, 44–61.
Overpeck, J.T., Webb III, T., Prentice, I.C., 1985. Quantitative interpretation of fossil pollen spectra: dissimilarity coefficients and the method of modern analogs. Quat. Res. 23, 87–108.
Peltier, W.R., Fairbanks, R.G., 2006. Global glacial ice volume and last glacial maximum duration from an extended Barbados sea level record. Quat. Sci. Rev. 25, 3322–3337.
Poulter, B., Pederson, N., Liu, H., Zhu, Z., D'Arrigo, R., Ciais, P., Davi, N., Frank, D., Leland, C., Myneni, R., Piao, S., Wang, T., 2013. Recent trends in Inner Asian forest dynamics to temperature and precipitation indicate high sensitivity to climate change. Agric. For. Meteorol. 178–179, 31–45.
Prentice, I.C., 1980. Multidimensional scaling as a research tool in quaternary palynology: a review of theory and methods. Rev. Palaeobot. Palynol. 31, 71–104.
Prentice, I.C., Cramer, W., Harrison, S.P., Leemans, R., Monserud, R.A., Solomon, A.M., 1992. A global biome model based on plant physiology and dominance, soil properties and climate. J. Biogeogr. 19, 117–134.
R Core Team, 2012. R: a Language and Environment for Statistical Computing. R Foundation for Statistical Computing, Vienna.
Raddatz, T.J., Reick, C.H., Knorr, W., Kattge, J., Roeckner, E., Schnur, R., Schnitzler, K.-G., Wetzel, P., Jungclaus, J., 2007. Will the tropical land biosphere dominate the climate–carbon cycle feedback during the twenty-first century? Clim. Dyn. 29, 565–574.
Ren, G.Y., 2007. Changes in forest cover in China during the Holocene. Veg. Hist. Archaeobot. 16, 119–126.
Roeckner, E., Bäuml, G., Bonaventura, L., Brokopf, R., Esch, M., Giorgetta, M., Hagemann, S., Kirchner, I., Kornblueh, L., Manzini, E., Rhodin, A., Schlese, U., Schultzweida, U., Tompkins, A., 2003. The Atmospheric General Circulation Model ECHAM5. Part I: Model Description. Max Planck Institut für Meteorologie, Hamburg. Report No. 349.
Shen, J., Liu, X., Wang, S., Matsumoto, R., 2005. Palaeoclimatic changes in the Qinghai Lake area during the last 18,000 years. Quat. Int. 136, 131–140.
Shi, Y., Zheng, B., Yao, T., 1997. Glaciers and environments during the Last Glacial Maximum (LGM) on the Tibetan Plateau. J. Glaciol. Geocryol. 19, 97–113 (in Chinese, with English Abstract).
Shi, Y.F., 2005. The Quaternary Glaciations and Environmental Variations in China. Hebei Science and Technology Press, Shijiazhuang, China (in Chinese).
Stebich, M., Rehfeld, K., Schütz, F., Tarasov, P.E., Liu, J., Mingram, J., 2015. Holocene vegetation and climate dynamics of NE China based on the pollen record from Sihailongwan Maar Lake. Quat. Sci. Rev. 124, 275–289.
Sugita, S., 1993. A model of pollen source area for an entire lake surface. Quat. Res. 39, 239–244.
Sun, Q.L., Zhou, J., Shen, J., Chen, P., Wu, F., Xie, X.P., 2006. Environmental characteristics of mid-Holocene recorded by lacustrine sediments from Lake Daihai, north environment sensitive zone, China. Sci. China Ser. D Earth Sci. 49, 968–981.
Svendsen, J.I., Alexanderson, H., Astakhov, V.I., Demidov, I., Dowdeswell, J.A., Funder, S., Gataullin, V., Henriksen, M., Hjort, C., Houmark-Nielsen, M., Hubberten, H.W., Ingólfsson, Ó., Jakobsson, M., Kjær, K.H., Larsen, E., Lokrantz, H., Lunkka, J.P., Lysså, A., Mangerud, J., Matiouchkov, A., Murray, A., Möller, P., Niessen, F., Nikolskaya, O., Polyak, L., Saarnisto, M., Siegert, C., Siegert, M.J., Spielhagen, R.F., Stein, R., 2004. Late quaternary ice sheet history of Northern Eurasia. Quat. Sci. Rev. 23, 1229–1271.
Tarasov, P., Williams, J.W., Andreev, A., Nakagawa, T., Bezrukova, E., Herzschuh, U., Igarashi, Y., Müller, S., Werner, K., Zheng, Z., 2007. Satellite- and pollen-based quantitative woody cover reconstructions for northern Asia: verification and application to late-quaternary pollen data. Earth Planet. Sci. Lett. 264, 284–298.
Tarasov, P.E., Volkova, V.S., Webb III, T., Guiot, J., Andreev, A.A., Bezusko, L.G., Bezusko, T.V., Bykova, G.V., Dorofeyuk, N.I., Kvavadze, E.V., Osipova, I.M., Panova, N.K., Sevastyanov, D.V., 2000. Last glacial maximum biomes reconstructed from pollen and plant macrofossil data from Northern Eurasia. J. Biogeogr. 27, 609–620.
Telford, R.J., Birks, H.J.B., 2011. Effect of uneven sampling along an environmental gradient on transfer-function performance. J. Paleolimnol. 46, 99–106.
ter Braak, C.J.F., Juggins, S., 1993. Weighted averaging partial least squares regression (WA-PLS): an improved method for reconstructing environmental variables from species assemblages. Hydrobiologia 269/270, 485–502.
Tian, F., Herzschuh, U., Telford, R.J., Mischke, S., Van der Meeren, T., Krengel, M., 2014. A modern pollen–climate calibration set from central-western Mongolia and its application to a late glacial–Holocene record. J. Biogeogr. 41, 1909–1922.
Wang, T., Wu, W., Xue, X., Sun, Q., Chen, G., 2004. Study of spatial distribution of sandy desertification in North China in recent 10 years. Sci. China Ser. D Earth Sci. 44 (Suppl. I), 78–88.
Wang, Y., Cheng, H., Edwards, R.L., Kong, X., Shao, X., Chen, S., Wu, J., Jiang, X., Wang, X., An, Z., 2005. Millennial- and orbital-scale changes in the East Asian monsoon over the past 224,000 years. Nature 451, 1090–1093.
Wang, Y., Herzschuh, U., Shumilovskikh, L.S., Mischke, S., Birks, H.J.B., Wischnewski, J., Böhner, J., Schlütz, F., Lehmkuhl, F., Diekmann, B., Wünnemann, B., Zhang, C., 2014. Quantitative reconstruction of precipitation changes on the NE Tibetan Plateau since the last glacial maximum – extending the concept of pollen source area to pollen-based climate reconstructions from large lakes. Clim. Past 10, 21–39.
Wang, Y., Liu, X., Herzschuh, U., 2010. Asynchronous evolution of the Indian and East Asian summer monsoon indicated by Holocene moisture patterns in monsoonal Central Asia. Earth Sci. Rev. 103, 135–153.
Williams, J.W., 2003. Variations in tree cover in North America since the last glacial maximum. Glob. Planet. Change 35, 1–23.
Williams, J.W., Jackson, S.T., 2003. Palynological and AVHRR observations of modern vegetational gradients in eastern North America. Holocene 13, 485–497.
Williams, J.W., Shuman, B., 2008. Obtaining accurate and precise environmental reconstructions from the modern analog technique and North American surface pollen dataset. Quat. Sci. Rev. 27, 669–687.
Williams, J.W., Tarasov, P., Brewer, S., Notaro, M., 2011. Late Quaternary variations in tree cover at the northern forest-tundra ecotone. J. Geophys. Res. 116, G01017. http://dx.doi.org/10.1029/2010JG001458.
Xiao, J.L., Xu, Q.H., Nakamura, T., Yang, X.L., Liang, W.D., Inouchif, Y., 2004. Holocene vegetation variation in the Daihai Lake region of north-central China: a direct indication of the Asian monsoon climatic history. Quat. Sci. Rev. 23, 1669–1679.
Xu, Q.H., Li, Y.C., Yang, X.L., Zheng, Z.H., 2007. Quantitative relationship between pollen and vegetation in northern China. Sci. China Ser. D Earth Sci. 50, 582–599.
Xu, Q.H., Tian, F., Bunting, M.J., Li, Y.C., Ding, W., Cao, X.Y., He, Z.G., 2012. Pollen source areas of lakes with inflowing rivers: modern pollen influx data from Lake Baiyangdian, China. Quat. Sci. Rev. 37, 81–91.
Yu, S.Y., 2013. Quantitative reconstruction of mid- to late-Holocene climate in NE China from peat cellulose stable oxygen and carbon isotope records and mechanistic models. Holocene 23, 1507–1516.
Yuan, D., Cheng, H., Edwards, R.L., Dykoski, C.A., Kelly, M.J., Zhang, M., Qing, J., Lin, Y., Wang, Y., Wu, J., Dorale, J.A., An, Z., Cai, Y., 2004. Timing, duration, and transitions of the last interglacial Asian monsoon. Science 304, 575–578.
Zheng, Y., Zheng, Z., Tarasov, P., Qian, L., Huang, K., Wei, J., Luo, C., Xu, Q., Lu, H., Luo, Y., 2010. Palynological and satellite-based MODIS observations of modern vegetational gradients in China. Quat. Int. 218, 190–201.
Zheng, Z., Deng, Y., Zhang, H., Yu, R.C., Chen, Z.X., 2004. Holocene environmental changes in the tropical and subtropical areas of the South China and the relation to human activities. Quat. Sci. 24, 387–393 (in Chinese, with English Abstract).
Zhu, Y., Xie, Y., Cheng, B., Chen, F., Zhang, J., 2003. Pollen transport in the Shiyang River drainage, arid China. Chin. Sci. Bull. 48, 1499–1506.